Drug Delivery and Translational Research (2022) 12:1697–1710
https://doi.org/10.1007/s13346-021-01068-4

ORIGINAL ARTICLE

A numerical study of the distribution of chemotherapeutic drug carmustine in brain glioblastoma

Hongyu Chen[1] · Guanghui Hu[1] · Defang Ouyang[2,3]

Accepted: 10 September 2021 / Published online: 14 October 2021

Abstract

To cure the illness in the brain glioblastoma, the Gliadel wafer, as the first FDA-approved chemotherapy, was available on the market since 1997. Due to the complex studies in vivo, more and more researchers have paid their attention to investigate the dynamic process in the brain by numerical methods. This study aimed to simulate the drug concentration in the cavity after drug releases from Gliadel wafers into the brain tumor by a two-dimensional simulation. The government equations, the parameters, and corresponding initial and boundary conditions are specified. Then the models are discretized and solved by finite element method (FEM) and finite difference method (FDM) based on C++ library Adaptive Finite Element Package (AFEPack) and MATLAB, respectively. First of all, the numerical convergence of the method is studied by numerical results represented in several successively refined meshes, which shows the reliability of our method. In the results from FEM, a steady state of the pressure in the normal tissue can be simulated. As for FDM, the changes of drug concentration are displayed at six different times. The numerical method in this paper is an effective tool for the numerical study on drug release from polymers. Additionally, convection is a critical factor in drug transportation. Moreover, the simulation approach can be used as the guild for remedy optimization and dynamic analysis of other drugs (paclitaxel) for tumor treatment in the clinic. This mathematical model has wide applications about drug release in multiple dosage forms, such as long sustained release microspheres, oral extended release hydrophilic matrix tablets, hydrogel, and sustained release topical rings.

Keywords Numerical model · Drug release · Convection · Brain tumor · Gliadel Wafer · AFEPack

Introduction

In 2016, 320000 new cases and 220000 death of central nervous system tumors in the USA were reported by the University of Washington [1]. The main brain tumors consist of neurogliomas (about 50%), pituitary tumors (about 15%), meningiomas (about 21%), and schwannomas (about 8%) [2]. As for diagnosis, most tracers may reach tumors in the body very optionally when there is a rupture from the blood–brain barrier (BBB), where BBB is the site that drugs can be controlled restrictively to pass. So the fracture of the BBB can be examined by magnetic resonance imaging (MRI) and computed tomography (CT), which are two popular diagnostic pointers for brain tumors [3]. For this treatment, surgical operation, radiotherapy, and chemotherapeutics will be combined and against cancers [4].

Gliadel wafer is the first FDA-approved chemotherapy to cure brain tumors in 1996 [5]. The whole weight of this wafer is 200mg, with a thickness of 1mm and a diameter of 14.5mm, which can be inserted into the cavity at the location where the tumor had been partly excised in surgery. In the center of residual brain tumor, the average implantation of eight wafers sustainedly releases carmustine at a dosage of 61.6mg, bypassing the BBB [6, 7]. Before 2010, BCNU (carmustine) wafers were approved as an appurtenance to surgical operation and radiation therapy in sufferers against neurogliomas and recrudescent glioblastoma multiforme [8]. Comparing to systemic chemotherapy, this treatment, which avoids repetitive injections and keeps a high local concentration in the target site, makes an extended survival time [9]. In one clinical test, four patients have been implanted with

✉ Guanghui Hu
garyhu@um.edu.mo

✉ Defang Ouyang
defangouyang@um.edu.mo

[1] Faculty of Science and Technology (FST), University of Macau, Macau, China

[2] State Key Laboratory of Quality Research in Chinese Medicine, Institute of Chinese Medical Sciences (ICMS), University of Macau, Macau, China

[3] Department of Public Health and Medicinal Administration, Faculty of Health Sciences (FHS), University of Macau, Macau, China

BCNU wafer to treat glioblastoma multiforme, and the survival time is in the range of 14 to 33 months, which is longer than the average of nearly 15 months as the survival time reported in another clinical test by the European Organisation Research and Treatment of Cancer (EORTC). In order to improve the opportunity of favorable patient results, clinicians sometimes combine BCNU wafers with other radiotherapies and chemotherapies [8], because the experimental tools are difficult to measure drug distribution in tumor sites. However, numerical methods are able to simulate the drug release process from the injection site to the tumors [10].

Simulation researches for this are sharply rising in recent years. Saltzman and Radomsky [11] initially built a one-dimensional model to research the agent distributed and eliminated in the brain when the drug release from a polymer. Fung et al. [12] illustrated the spatial distribution of BCNU, containing the amount and concentration of drugs nearby the polymer implants upon a one-month period in the rat brain. Kalyanasundaram et al. [13] added FEM and construct a two-dimensional (2D) model to predict the agent distribution delivered to a rabbit brain. Wang et al. [14] and Tan et al. [15] updated the abstract model via three-dimensional human brain tumors and added the convection influences which could be significant after surgery. Arifin et al. [6, 7] constructed an ordinary differential equation (ODE) model, which assumed that the concentration is not related to time steps. In summary, all of the preceding studies offered advantageous knowledge for better therapeutics against brain tumors, emphasizing the contribution of mathematical simulation. Sometimes, combining the numerical methods in partial differential equations (PDEs) with the ODE system may describe the systemic model precisely. Actually, ODE is always considered the single variable or parameter, which can show some specific mechanisms, but it may lack the component of the dynamics in the spatial region of the tumor if the PDE is neglected [16].

The purpose of this study is mainly to do the two-dimensional PDE model for pressure in the brain tissue and carmustine releasing from Gliadel® wafers by numerical methods. To simplify the study, the domain of this problem used for modeling brain and tumor should be a bounded one, and it is restricted from R^3 to R^2, which stands for a slice of the brain . The drug release is researched inside the brain slice because the reduction of the dimension will significantly simplify the study to explain some potential phenomena. First method is the FEM, which is a modern computational method that is used for solving problems in the mathematical models. Here, a mass continuity equation, a constitutive equation, and a simple momentum equation in the brain tissue are integrated into a new elliptic equation that contains an unknown variable (pressure in the interstitial fluid) and can be discretized into a system of matrix formulation. In detail, this large system will be subdivided into smaller portions that are called finite elements. This can be attained by a special space discretization in the spatial dimensions, which is performed by the building of a mesh of the model geometry: a finite number of points will be contained in the giving domain for the numerical solution. The form of a boundary value problem finally converts to a system of algebraic equations, and then they are approximated by the unknown function in the domain. Since the practical problems in brain tissue are difficult to obtain accurate solutions, the variational methods will be utilized from the variable calculus to approximate a solution by minimizing an associated error function. After the discretization, the corresponding codes will be written into a flexible and general computer program AFEPack [17]; this package is actually a library of classes for finite element processing. Next, the numerical solution in every discretized point can be displayed by a visual software Open Data Explorer (OpenDX) which is able to handle the complex domains (like the human brain) along with measured or computed data. Afterward, the details of the simulation result will be obtained. Second is the FDM, and this numerical method is a direct way for solving PDE by approximating derivatives with finite differential. In this research, the given conservation equation of the concentration is the standard formulation of the diffusion–convection–reaction equation. After simplifying the equation in the cavity and the computational domain by a regular shape, the modified PDE will be discretized, or subdivided into a finite number of steps, then it is converted into a system of linear equations, and the solution value is approximated by solving the algebraic equations at those discrete points. Subsequently, the relevant codes will be created and compiled with the discretizing equation in MATLAB. Also, the effect of the convection flow is considered in an ODE model, following the former research in the references [6, 7] with some modifications. Moreover, by comparing the experimental data with the numerical results, it is captured that convection is significant and these methods can be utilized on other potential models, such as sustained release microspheres and oral extended release hydrophilic matrix tablets, for the further studies.

Models and methodologies

Mathematical model

The information of the tumor model is from [6]. The geometry of a patient brain tumor was acquired from MRI. This procedure could rebuild the brain geometry precisely of $+/-$ 3 mm. The volume of the concrete tumor is 12.8 cm^3, with an average radius (R) of this sphere of 14.5 mm. After complete tumor resection, the tumor remains about 60% of an open cavity in the center part and the equivalent thickness (L) of the

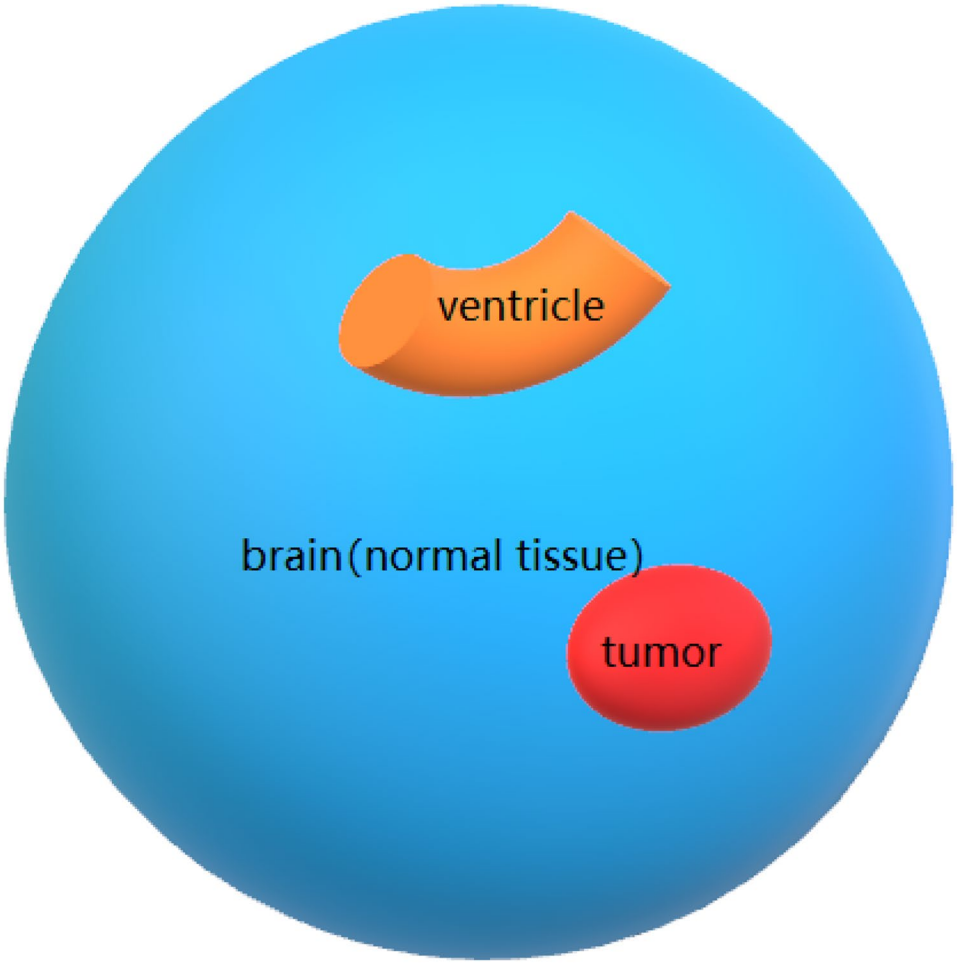

Fig. 1 The model geometry of the brain, showing the presence of ventricle (the brown part), tumor (red part), and rest is the normal brain tissue

left tumor is around 2.3 *mm* around the leftover tumor. Afterward, eight wafers will be implanted in the cavity by Surgical cellulose [6, 7]. Figure 1 shows the site of the ventricle and brain tumor in the brain. Figure 2 portrays a simple image performance with a cut section of the brain. $\partial\Omega_1$, $\partial\Omega_2$, $\partial\Omega_3$ are the different domain boundaries. Domain Ω_1 shows the normal tissue of the brain, domain Ω_2 delineates the remnant tumor part which is remained from the surgical operation, the portion of the excision cavity is shown in the domain Ω_3, and in the most inner domain Ω_4, there are the eight Gliadel wafer implants.

Transport equations

In this research, the brain tumor is dealt with as a spatially homogeneous domain, due to the absence of in vivo data to demonstrate the heterogeneous distribution. The mass continuity equation in the interstitial space for the normal tissue can be expressed as:

$$\nabla \cdot \mathrm{v} = \mathrm{F_{bv}}, \tag{1}$$

where v is velocity vector in the interstitial space, $\mathrm{F_{bv}}$ represents the change of net fluid flow obtained from capillary in the blood circulation system. It also satisfies Starling's law:

$$\mathrm{F_{bv}} = \mathrm{L_{bv}} \frac{\mathrm{S}}{\mathrm{V}} \left[\mathrm{p_{bv}} - \mathrm{p_{in}} - \sigma_{\mathrm{T}}\left(\pi_{\mathrm{bv}} - \pi_{\mathrm{in}}\right)\right], \tag{2}$$

Here, $\mathrm{L_{bv}}$ is the hydraulic conductivity from the vascular wall, S is the vascular surface area, and V is the parallel volume in the normal tissue. $\mathrm{p_{bv}}$ and $\mathrm{p_{in}}$ are the pressure in the blood vessel and interstitial space, respectively. π_{bv} is the osmotic pressure in the vascular space, and π_{in} is the interstitial space osmotic pressures. σ_{T} is the coefficient of osmosis reflection for the plasma proteins [18]. In the brain, due to the absence of lymphatic vessels by functional operation, the fluid loss in the lymphatic system can be neglected [19].

Both the normal tissue and brain tumor are regarded as a porous medium that satisfies Darcy's law, because of drug transportation scale is not always shorter than the distance among the capillaries [20, 21].

The expression form of mathematical equation about this phenomenon is:

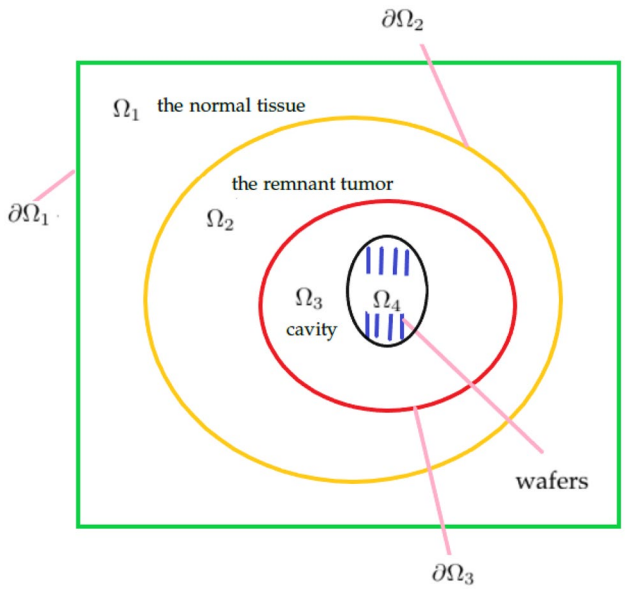

Fig. 2 The model of the tumor in the brain. The region Ω_1 – the normal tissue, Ω_2 – the remnant tumor, Ω_3 – the cavity. The boundary $\partial\Omega_1$ – the external boundary, $\partial\Omega_2$ – boundary between residual tumor and brain normal tissues, $\partial\Omega_3$ – boundary between the cavity and residual tumor. Ω_4 represents the wafer area. Eight blue lines represent the eight Gliadel wafers in the center of the cavity

$$\rho\left(\frac{\partial \mathrm{v}}{\partial \mathrm{t}}+\mathrm{v}\cdot\nabla\mathrm{v}\right)=-\nabla \mathrm{p_{in}}+\mu\nabla^2\mathrm{v}+\frac{\mu}{\mathrm{K}}\mathrm{v}, \tag{3}$$

where ρ and μ are the interstitial space density and interstitial space viscosity, respectively. K is the normal tissue permeability , and t is time [22].

The velocity in the interstitial fluid could be further rewrite by the direct proportion of pressure gradient because of the Darcy's law [6, 7, 14, 23]:

$$\mathrm{v}=-\frac{\mathrm{K}}{\mu}\nabla \mathrm{p_{in}}, \tag{4}$$

then a steady equation can be solved [24] by combining Eqs. (1), (2) and (4):

$$\nabla^2\mathrm{p_{in}}=\frac{\mu}{\mathrm{K}}\mathrm{L_{bv}}\frac{\mathrm{S}}{\mathrm{V}}\mathrm{p_{in}}-\frac{\mu}{\mathrm{K}}\mathrm{L_{bv}}\frac{\mathrm{S}}{\mathrm{V}}[\mathrm{P_{bv}}-\sigma_{\mathrm{T}}(\pi_{\mathrm{bv}}-\pi_{\mathrm{in}})]. \tag{5}$$

The dimensionless modalities of mass continuity and motion equations could be shown to:

$$\tilde{\nabla}\cdot\tilde{\mathrm{v}}=\tilde{\mathrm{F}}_{\mathrm{bv}}, \tag{6}$$

$$\frac{\partial\tilde{\mathrm{v}}}{\partial\tau}+\tilde{\mathrm{v}}\cdot\tilde{\nabla}\tilde{\mathrm{v}}=-\frac{(\mathrm{p_v}-\mathrm{p_o})}{\rho\mathrm{v_c^2}}\tilde{\nabla}\tilde{\mathrm{p}_{\mathrm{in}}}+\frac{1}{\mathrm{Re}}\tilde{\nabla}^2\tilde{\mathrm{v}}-\frac{1}{\mathrm{Re}}(\frac{\mathrm{L_b^2}}{\mathrm{K}})\tilde{\mathrm{v}}, \tag{7}$$

where $\tilde{\nabla}=\mathrm{L_{br}}\nabla$ and $\mathrm{L_{br}}$ is the brain average radius. $\tilde{\mathrm{v}}=\mathrm{v}/\mathrm{v_c}$, here $\mathrm{v_c}$ is the scalar velocity in the interstitial space, i.e. $1\times10^{-7}\ m/s$ in the brain tissue. $\mathrm{p_v}$ and $\mathrm{p_o}$ are the pressure from ventricle part and normal tissue domain, respectively, and $\widetilde{\mathrm{p}}_{\mathrm{in}}=\left(\mathrm{p_{in}}-\mathrm{p_0}\right)/\left(\mathrm{p_v}-\mathrm{p_0}\right)$ is the dimensionless pressure [7]. τ is the dimensionless time, and the form of $\mathrm{Re}=\rho\mathrm{L_b}\mathrm{v_c}\mu^{-1}$ is Reynolds number.

In the normal tissue, drugs could be divided into two various forms as free (F) and bound (B). Moreover, brain normal tissue is constituted by three compartments: cell membrane(CM), extracellular/interstitial space (ES), and intracellular space (IS). Only drugs in free form could cross through the CM into the interior space [25]. The drug transport among three compartments is graphically depicted in Fig. 3.

The drug concentration in both two forms can be described by:

$$\begin{aligned}F&=\alpha F_{ES}+\beta F_{IS}+(1-\alpha-\beta)F_{CM}\\B&=\alpha B_{ES}+\beta B_{IS}+(1-\alpha-\beta)B_{CM},\end{aligned} \tag{8}$$

Here, α is the extracellular spaces volume fraction, and β is the cell interior volume fraction. Due to there is no elimination or bound effect between drugs and proteins on cytomembrane, B_{CM}, the equivalent agent concentration in bounded state, is assumed to be 0 [25].

In extracellular space, the availability of the free drug is related to drug transport by diffusion, convection, metabolism, and local proteins binding. Then the drug concentration equation could be demonstrated by:

$$\frac{\partial F}{\partial t}=\alpha D_{ES}\nabla^2F_{ES}-\nabla\cdot\left(vF_{ES}\right)-\alpha\left(k_{bbb}+k_e\right)F_{ES}-\beta k_eF_{IS}-\frac{\partial B}{\partial t}, \tag{9}$$

where D_{ES} is agent diffusivity in the extracellular space, t is time, k_{bbb} is the elimination constant for agent passing the BBB, k_e is the elimination velocity because of reactions by enzymatic and non-enzymatic processes. By presuming the linear relationship of free and bound drugs concentration [6, 7, 26], and the equivalence of free drugs among ES, CM, and IS, $(P_{IS-ES}=F_{IS}/F_{ES};P_{CM-ES}=F_{CM}/F_{ES})$ [11, 22, 27],

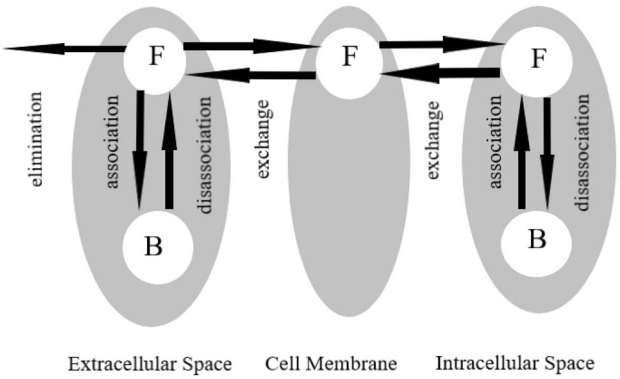

Fig. 3 The situation for drug transport in ES, CM, and IS

Table 1 Parameters in the brain tissues

Symbol	Parameter	Cavity	Remnant tumor	Normal tissue	Source
F_{bv}	Hydraulic conductivity ($m/Pa/s$)	N/A	1.1×10^{-12}	1.4×10^{-13}	Arifin et al. [7]
α	Volume fraction of interstitial fluid	1	3.5×10^{-1}	2×10^{-1}	Fung et al. [12]; Kalyanasundaram et al. [13]
β	Volume fraction of intracellular space	0	5.5×10^{-1}	6.5×10^{-1}	Fung et al. [12]; Kalyanasundaram et al. [13]
ρ	Density in the extracellular space (kg/m^3)	1×10^3	1×10^3	1×10^3	Green and Perry [32]
μ	Viscosity in the extracellular space ($kg/m/s$)	7×10^{-4}	7×10^{-4}	7×10^{-4}	Green and Perry [32]
p_{bv}	Pressure in blood vessel (Pa)	N/A	4.61×10^3	4.61×10^3	Kimelberg [33]
p_v	Pressure at the ventricle (Pa)	1.4474×10^3	1.4474×10^3	1.4474×10^3	Kimelberg [33]
p_o	Pressure at outer phase (Pa)	6.579×10^2	6.579×10^2	6.579×10^2	Kimelberg [33]
$\frac{S}{V}$	Surface area of vascular blood per tissue volume (m^{-1})	N/A	2×10^4	7×10^3	Baxter and Jain [20]
π_{bv}	Osmotic pressure in the blood vessel (Pa)	N/A	3.44×10^3	3.44×10^3	Kimelberg [33]
π_{in}	Osmotic pressure in the interstitial fluid (Pa)	N/A	1.11×10^3	7.4×10^2	Baxter and Jain [20]
σ_T	Osmotic coefficient of blood tissue	N/A	8.2×10^{-1}	9.1×10^{-1}	Baxter and Jain [20]
K	Darcy permeability (m^2)	1.0×10^{-11}	6.4×10^{-14}	6.4×10^{-15}	Arifin et al. [7]

the agent concentration equation is the simplified form as follow:

$$\frac{\partial F_{ES}}{\partial t} = D^* \nabla^2 F_{ES} - v^* \cdot \nabla F_{ES} - k^* F_{ES}, \tag{10}$$

Here, $\alpha^* = \alpha\left(1 + K_{ES}\right) + \beta P_{IS-ES}\left(1 + K_{IS}\right) + (1 - \alpha - \beta)P_{CM-ES}$ is a parameter value that reflects the agent capacities of local binding and cell membrane partitioning, $v^* = v/\alpha^*$ is the apparent velocity in the extracellular space, and $D^* = (\alpha/\alpha^*)D_{ES}$ is the agent apparent diffusion coefficient in brain tissue. $k^* = \left[ak_{bbb} + (a + \beta)k_e + F_v\right]/\alpha^*$ is the apparent elimination constant [7, 27].

In the cavity, carmustine is in the interstitial fluid for transport. Diffusion and convection can influence without any limitations due to the local binding with proteins and cell membrane partitioning can be ignored. Therefore, the diffusion–convection–reaction equation of drug distribution in the extracellular space can be described by the following:

$$\frac{\partial F_{ES}}{\partial t} = D_{ES} \nabla^2 F_{ES} - v \cdot \nabla F_{ES} - k_c F_{ES}, \tag{11}$$

where v is the velocity vector in the extracellular space and could be calculated by the Eq. (4) [6], and k_c is the elimination parameter in the open cavity [28].

Parameters

Summarized in two tables, Tables 1 and 2 provide the equation parameter values related to the brain tissue, and anticancer drugs [29]. In human brain, the entire flow speed of interstitial fluid is approximately 5.83×10^{-6} kg/s [30, 31]. The initial concentration is assumed to

Table 2 Parameter values about carmustine

Symbol	Parameter	Carmustine	Source
MW	Molecular mass (g/mol)	$2.14 \times 1o^2$	Wolff et al. [34]
D_{ES}	Diffusion coefficient in the extracellular space (m^2/s)	1.5×10^{-9}	Fung et al. [12]
P_{IS-ES}	Distribution coefficient between cellular and interstitial fluid	1	Fung et al. [12]
P_{CM-ES}	Distribution coefficient between cell membrane and interstitial fluid	1.03×10^2	Fung et al. [12]
K_{ES}, K_{IS}	Binding constant of free and bound agent in the extracellular and intracellular fluid	5.0	Fung et al. [12]
k_{bbb}	Drug elimination from microvascular bed ($1/s$)	1.4×10^{-2}	Fung et al. [12]
k_e	Drug elimination because of reactions by enzymatic/non-enzymatic process($1/s$)	1.1×10^{-4}	Fung et al. [12]
k_c	Cavity elimination constant($1/s$)	9.63×10^{-5}	Fleming and Saltzman [35]
$F_{ES,eff}$	Effective therapy of concentration (kg/m^3)	3.2×10^{-3}	Fung et al. [25]

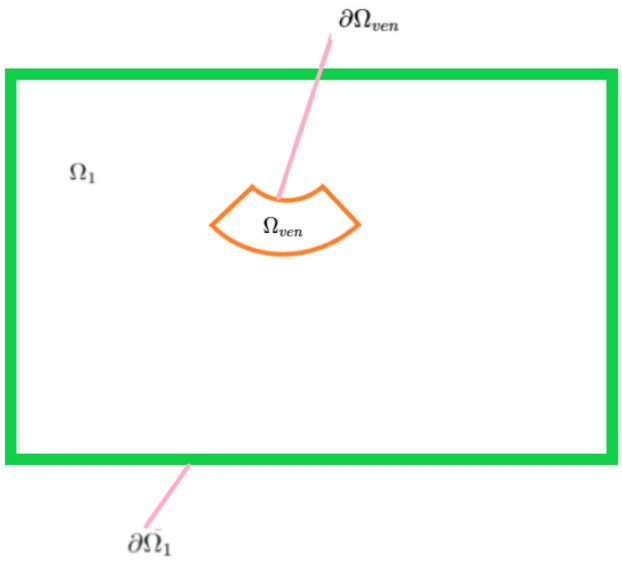

Fig. 4 The model of the ventricle. The region Ω_1– the normal tissue, The region Ω_{ven}– the ventricle surface, The boundary $\partial\Omega_1$– the external boundary, $\partial\Omega_{ven}$– boundary on the ventricle part

be 0.05 kg/m^3 due to the ratio of dosage of carmustine in each wafer to the volume of the cavity by surgically removed.

Numerical methods

The method on interstitial pressure

The mathematical model about the p_{in} distribution in the brain is based on AFEPack and FEM, Aiming at the Eq. (5), discretization is necessary by using the Ritz-Galerkin method. A simple picture about the boundary and domain can be showed by Fig. 4.

Here we let

$$u = \mathrm{p_{in}},$$

$$a_1 = \frac{\mu}{\mathrm{K}}\mathrm{L_{bv}}\frac{\mathrm{S}}{\mathrm{V}},$$

$$b_1 = \frac{\mu}{\mathrm{K}}\mathrm{L_{bv}}\frac{\mathrm{S}}{\mathrm{V}}[\mathrm{P_{bv}} - \sigma_{\mathrm{T}}(\pi_{\mathrm{bv}} - \pi_{\mathrm{in}})],$$

then Eq. (5) can be written as follow:

$$\nabla^2 u = a_1 u - b_1 \quad \text{in} \quad \Omega_1, \tag{12}$$

$$u(x, y) = 1447.4 \quad \text{on} \quad \partial\Omega_{ven}, \tag{13}$$

$$u(x, y) = 657.9 \quad \text{on } \partial\Omega_1, \tag{14}$$

where Ω_1 is the open boundary about the normal brain, with a piecewise and smooth boundary $\partial\Omega_1$, $\overline{\Omega} = \Omega_1 \cup \partial\Omega_1$.

If $U \in H^1(\Omega_1) \times H^1(\Omega_1)$ is a vector in 2D, then

$$\iint_{\Omega_1} \mathrm{div}\ U dxdy = \iint_{\Omega_1} \nabla \cdot U dxdy = \int_{\partial\Omega_1} U \cdot \mathrm{n} dr, \tag{15}$$

where $H^1(\Omega_1)$ a Hilbert space, n is the unit normal vector which points at the boundary $\partial\Omega_1$, and dr is a line element.

Let $U = v\nabla u = \left[v\frac{\partial u}{\partial x}, v\frac{\partial u}{\partial y}\right]^T$, then

$$\begin{aligned}\iint_{\Omega_1} \nabla \cdot \mathrm{U} dxdy &= \iint_{\Omega_1} (v\Delta u + \nabla u \cdot \nabla v) dxdy \\ &= \int_{\partial\Omega_1} \mathrm{U} \cdot \mathrm{n} dr \\ &= \int_{\partial\Omega_1} v\nabla u \cdot \mathrm{n} dr = \int_{\partial\Omega_1} v\frac{\partial u}{\partial n} dr,\end{aligned} \tag{16}$$

where $\mathrm{n} = (n_x, n_y)(n_x^2 + n_y^2 = 1)$ is the unit normal vector, then $\frac{\partial u}{\partial n} = \nabla u \cdot \mathrm{n} = n_x\frac{\partial u}{\partial x} + n_y\frac{\partial u}{\partial y}$.

The format of a linear elliptic PDE in second order is

$$\begin{aligned}A(x, y)u_{xx} + 2B(x, y)u_{xy} + C(x, y)u_{yy} + D(x, y)u_x + E(x, y)u_y \\ + F(x, y) + G(x, y)u = 0\end{aligned} \tag{17}$$

the discriminant of this equation is $B^2 - AC < 0$. The format of a self-adjoint elliptic PDE in second order is

$$-\nabla \cdot (m(x, y)\nabla u) + n(x, y)u = F(x, y), \tag{18}$$

let $u(x, y) \in H^2(\Omega_1)$, $v(x, y) \in H^1(\Omega_1)$, then

$$\iint_{\Omega_1} v\Delta u dxdy = \int_{\partial\Omega_1} v\frac{\partial u}{\partial n} dr - \iint_{\Omega_1} \nabla u \cdot \nabla v dxdy. \tag{19}$$

Transforming the equation and adding an arbitrary test function $v(x, y) \in H^1(\Omega_1)$, then

$$\iint_{\Omega_1} (-\nabla^2 u) + a_1 u)v dxdy = \iint_{\Omega_1} b_1 v dxdy, \tag{20}$$

and utilizing the integration by parts then the equation will be as follow:

$$\iint_{\Omega_1} (\nabla u \cdot \nabla v + a_1 uv) dxdy - \int_{\partial\Omega_1} vu_n dr. \tag{21}$$

The weak form of this is

$$\begin{aligned}\iint_{\Omega_1} (\nabla u \cdot \nabla v + a_1 uv) dxdy = \iint_{\Omega_1} b_1 v dxdy \\ + \int_{\partial\Omega_N} g(x, y)v(x, y) dr \\ for\ \forall v(x, y) \in H^1(\Omega_1),\end{aligned} \tag{22}$$

here, $\partial\Omega_N$ is called as Neumann boundary condition.

The solution space of the above equations is

$$V = \{v(x,y),\ for\ v(x,y) = 0,\ and\ (x,y) \in \partial\Omega_D,\ for\ v(x,y) \in H^1(\Omega_1)\}, \tag{23}$$

here $\partial\Omega_D$ is Dirichlet boundary condition.

Then, the definition of the bilinear format is

$$B(u,v) = \iint_{\Omega_1} (\nabla u \cdot \nabla v + a_1 uv)dxdy, \tag{24}$$

and the linear form is

$$L(v) = \iint_{\Omega_1} b_1 v dxdy. \tag{25}$$

A basis function of the piecewise linear functions in $H^1(\Omega_1)$ can be defined as

$$\psi_i(x_j) = \begin{cases} 1, & \text{when } i = j; \\ 0, & \text{otherwise .} \end{cases} \tag{26}$$

Then

$$\psi_i \in V_h,\ \ U = \sum_{i=1}^{N} u_i\psi_i,\ \ u_i \text{ are unknown scalars,} \tag{27}$$

where $V_h = \{v(x,y)$ is continuous in Ω_1 and piecewise linear over each non-overlapping triangles $v(x,y)|_{\partial\Omega_1} = 0\}$.

$$v = \sum_{i=1}^{N} v_i\psi_i, \tag{28}$$

then

$$B\left(\sum_{j=1}^{N} \left(U_j\psi_j, \psi_i\right)\right) = L(\psi_i),\ j = 1, \ldots, N, \tag{29}$$

that is

$$\sum_{i=1}^{N}[(\nabla\psi_i, \nabla\psi_j) + (a_1\psi_i, \psi_j)]u_i = (b_1, \psi_j),\ j = 1, \ldots, N. \tag{30}$$

The method on concentration

The simulation of the concentration in cavity is supported by MATLAB via second-order FDM, and each term about discretization of the government equation is gained by the Euler method, first upwind scheme and second-order explicit scheme. Cavity is regarded as a square with length r_c is 8.7 *mm*. The agent concentration will be negligible in the Ω_1, Ω_2, Ω_3 at the initial condition.

Firstly we let

$$u = F_{ES},$$

$$a = D_{ES},$$

$$b = \text{v},$$

$$c = k_c$$

the next step is to choose integers $n = 64$ to define step size $h = (x_n - x_1)/n$, where x_n and x_1 are the end point and start point of given interval in x axis, respectively, and do the same as in y axis. k is time step size.

The Eq. (11) can be expressed by:

$$\frac{\partial u}{\partial t} = a\left(\frac{\partial^2 u}{\partial x^2} + \frac{\partial^2 u}{\partial y^2}\right) - b(u_x + u_y) - cu, \tag{31}$$

$$\frac{\partial u}{\partial t}(x_l, y_m, t_n) = \frac{1}{k}\left(u_{l,m}^{n+1} - u_{l,m}^{n}\right), \tag{32}$$

$$\begin{aligned} &a\left(\frac{\partial^2 u}{\partial x^2} + \frac{\partial^2 u}{\partial y^2}\right)(x_l, y_m, t_n) \\ &= \frac{a}{h^2}\left(u_{l-1,m}^{n} - 2u_{l,m}^{n} + u_{l+1,m}^{n} + u_{l,m-1}^{n} - 2u_{l,m}^{n} + u_{l,m+1}^{n}\right) \\ &= \frac{a}{h^2}\left(-4u_{l,m}^{n} + u_{l-1,m}^{n} + u_{l+1,m}^{n} + u_{l,m-1}^{n} + u_{l,m+1}^{n}\right), \end{aligned} \tag{33}$$

$$-b(u_x + u_y)(x_l, y_m, t_n) = -\frac{b}{h}\left(u_{l,m}^{n} - u_{l-1,m}^{n} + u_{l,m}^{n} - u_{l,m-1}^{n}\right), \tag{34}$$

$$-cu = -cu_{l,m}^{n}, \tag{35}$$

$$\begin{aligned} u_{l,m}^{n+1} &= u_{l,m}^{n} - cku_{l,m}^{n} + \frac{ak}{h^2}\left(-4u_{l,m}^{n} + u_{l-1,m}^{n} + u_{l+1,m}^{n} + u_{l,m-1}^{n} + u_{l,m+1}^{n}\right) \\ &\quad - \frac{bk}{h}\left(u_{l,m}^{n} - u_{l-1,m}^{n} + u_{l,m}^{n} - u_{l,m-1}^{n}\right) \\ &= \left(1 - ck - \frac{4ak}{h^2} - \frac{2bk}{h}\right)u_{l,m}^{n} + \left(\frac{ak}{h^2} + \frac{bk}{h}\right)\left(u_{l-1,m}^{n} + u_{l,m-1}^{n}\right) \\ &\quad + \frac{ak}{h^2}\left(u_{l+1,m}^{n} + u_{l,m+1}^{n}\right). \\ &\quad \text{(explicit scheme)} \end{aligned} \tag{36}$$

$$\begin{aligned} u_{l,m}^{n} &= \left(1 + ck + \frac{4ak}{h^2} + \frac{2bk}{h}\right)u_{l,m}^{n+1} - \left(\frac{ak}{h^2} + \frac{bk}{h}\right)\left(u_{l-1,m}^{n+1} + u_{l,m-1}^{n+1}\right) \\ &\quad - \frac{ak}{h^2}\left(u_{l+1,m}^{n+1} + u_{l,m+1}^{n+1}\right). \\ &\quad \text{(implicit scheme)} \end{aligned} \tag{37}$$

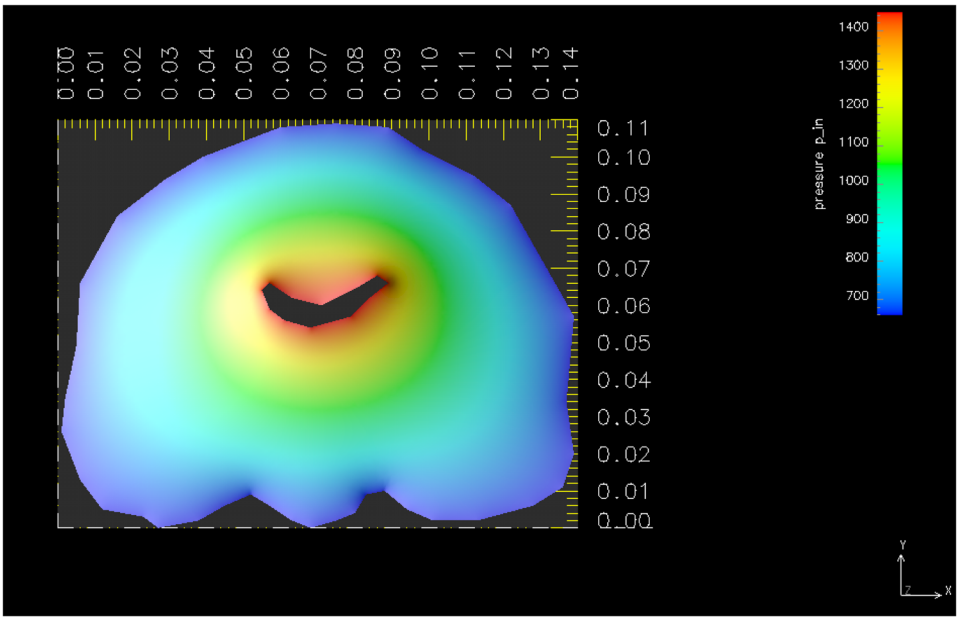

Fig. 5 The steady state of p_{in} contour on the surface of the brain

Boundary condition

The ventricle surface pressure and normal brain tissue pressure are chosen as 1447.4 *Pa* [33] and 657.9 *Pa* [36], respectively. All variables among the $\partial\Omega_1$, $\partial\Omega_2$, $\partial\Omega_3$ are presumed to be continuous.

Results and discussion

Numerical results of p_{in} distributed in the brain

Figure 5 displays the 2D distribution of the interstitial pressure around the ventricle to the whole brain, the high pressure is red surrounding the ventricle, which diffuses to the external environment of the brain. This is a steady situation in tumor, due to the simplification of **v** is not relevant with t in Eq. (4). In order to show the numerical convergence, a relatively dense mesh will be assumed as the analytic solution (after four times refinement), then by comparing the coarse mesh and the assumptive true solution, the L2-error and L1-error can be obtained by comparing the next mesh with the above one with their convergence rate. The refinements of mesh grids are shown in Fig. 6, and the meshes are more and more smooth because of the increase of elements, with the error in Table 3.

Numerical results of drug distribution in the cavity

Equation (9) has a dimensionless format, which could be transformed as

$$\frac{\partial \Gamma}{\partial \tau} = \widetilde{\nabla}^2 \Gamma - \mathrm{Pe}_c \widetilde{v} \cdot \widetilde{\nabla} \Gamma - \Gamma, \tag{38}$$

where $\Gamma = F_{ES}/F_{\mathrm{ES,eff}}$ is dimensionless agent concentration normalized to the effective therapy of concentration, $\tau = tk_c$ is the time in dimensionless form of the agent elimination due to degradation into the cavity, $L_c(= 1\ cm)$ is the length scale of the cavity size, $\widetilde{\mathrm{v}} = \mathrm{v}/\mathrm{v}_c$ is the dimensionless extracellular space velocity. In this simulation, $\mathrm{v} = 8 \times 10^{-7}\ m/s$ is volume-averaged velocity. $\mathrm{Pe}_c = \mathrm{v}_c L_c / D_{ES} = 2$ is a Peclet number that observes the significance of convection influence diffusion into the open cavity [6, 7]. $\xi_c = x_c/L_c$ is distance from cavity interface (x_c) normalized to the cavity size length scale (L_c).

Combining with the assumption in Subsection 2.4 and the concentration on boundary $\partial\Omega_3$ which is regarded to be 0, Fig. 7 reveals the numerical results of the dimensionless concentration Γ against to the dimensionless distance ξ_c. There are two significant messages which can be shown by the following pictures. Firstly, the carmustine concentration reaches effective therapeutic conditions ($\Gamma > 1$) nearly before 120h. After that, the drug dimensionless concentration decreases below the effective concentration ($\Gamma < 1$). Next, the loss of carmustine concentration in the cavity is mainly by the diffusion. Due to the coefficient of convection term v is assumed to be the average one, the influence of convection is showed by the concentration that shifts in the upper right corner. The domain is assumed to be a regular geometry, which shows the numerical results in this mesh after discretizing. The direction of the upper right means a specific trend primarily affected by the combination of diffusion, convection and reaction in this 2D plane. It depends

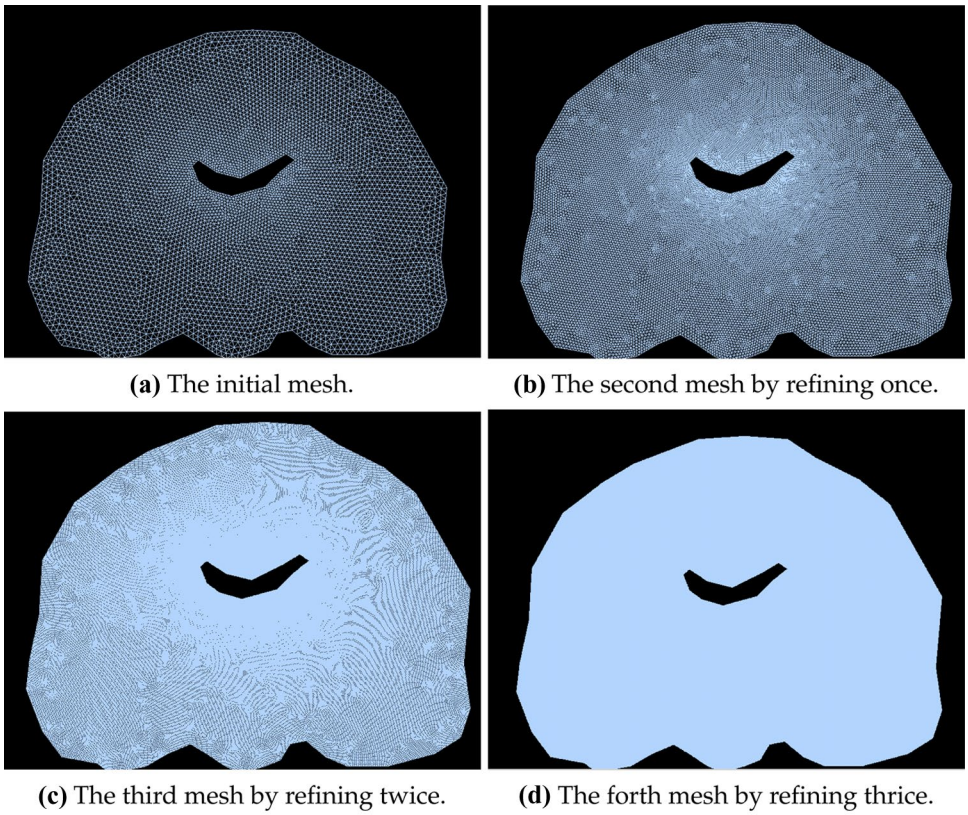

Fig. 6 Four successively refined mesh, with (**a**) 12028 elements, (**b**) 48112 elements, (**c**) 192448 elements, (**d**) 769792 elements

on the establishment of the coordinate system and the drug placement in the initial time., and the penetration to remnant tumor is limited, even at the start time when carmustine concentration is high in the cavity. The details of this are discussed in next section.

Approximately 120h is the period of the carmustine releasing in vivo; As for Gliadel wafers in the interstitial fluid, the period of complete degradation of this wafer is from 42 to 56 days, and the metabolic elimination studies have shown that the products of carmustine degradation are excreted mainly by urine [35], which is nearly anastomotic in the above simulation.

The reason that the FEM is not utilized on this diffusion–convection–reaction equation is that when the influence of convection is far greater than that of diffusion, it will bring many difficulties to the numerical solution, such as numerical oscillation and numerical excessive diffusion. Hence, to maintain the stability of the final results, FDM seems a satisfactory way to simulate the process. On the whole, the two numerical methods are feasible to estimate the different conditions in the brain tissue and to simulate the approximate results in the different parameters.

Table 3 The error and the convergence rate

dx	L2 Error Norm	$rate_2$	L1 Error Norm	$rate_1$
1/70	6.3e-2	1.41	4.1e-3	1.44
1/140	2.37e-2	1.49	1.5e-3	1.52
1/280	8.47e-3	1.81	5.27e-4	1.83
1/560	2.42e-3	-	1.48e-4	-

Drug penetration to the remnant tumor

To consider the influence of convection flow precisely, the hypothetical lines *I*, *II*, *III* will represent three different directions of convection flow. The diffusion permeates from cavity to remnant tumor because of the changes of concentration, which is on account of the gradient of the concentration. As a consequence, the convection flow inline *I* cooperates with diffusion, thereby enhancing the penetration. Along with *II* is the place where convection is neglectable due to it is vertical to the cavity surface. As for line *III*, convection restricts the effect of diffusion. Hence, in this region, the permeation is suppressed [7]. (see Fig. 8)

One simple preceding equation is analyzed under the assumption of quasi-steady conditions, which can be studied by:

$$0 = \frac{d^2\Gamma_t}{d\xi^2} - \mathrm{Pe}_t\left(\frac{v_x}{\mathrm{v}_c}\right)\frac{d\Gamma_t}{d\xi} - \Gamma_t, \tag{39}$$

where $\Gamma_t = F_{ES}/F_c$ is the dimensionless agent concentration uniformized to the interfacial surface between the open

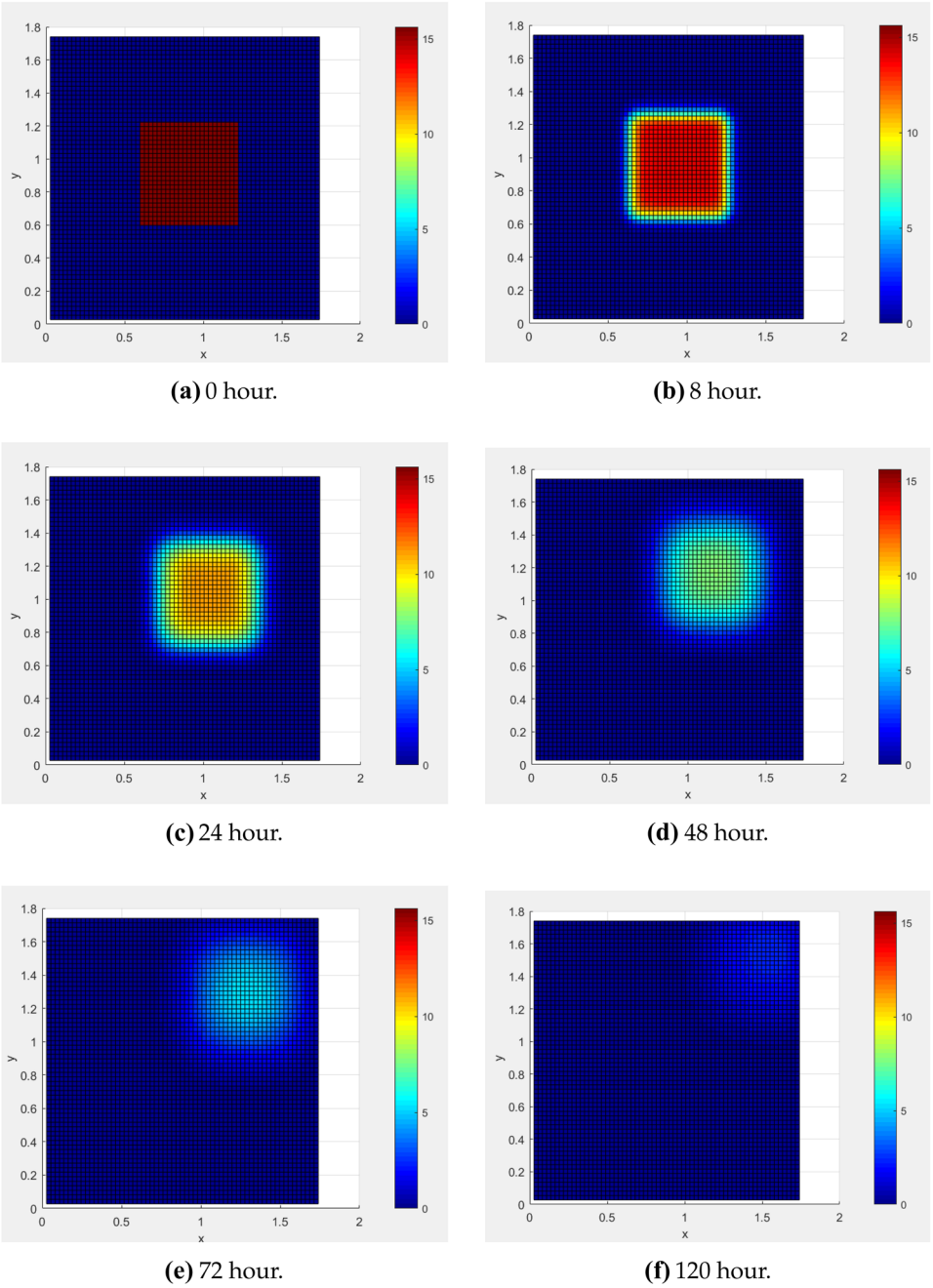

(a) 0 hour. **(b)** 8 hour. **(c)** 24 hour. **(d)** 48 hour. **(e)** 72 hour. **(f)** 120 hour.

Fig. 7 The contour dimensionless concentration on the cavity surface in six different times. (**a**) 0 hour, (**b**) 8 hour, (**c**) 24 hour, (**d**) 48 hour, (**e**) 72 hour, (**f**) 120 hour. x, y are both the dimensionless distance ξ_c in two directions. The changes of Γ are revealed by the color bar

cavity and remnant tumor, (F_c) and $\xi = x/L_t$ is the dimensionless distance from the interfacial surface between the open cavity and remnant tumor (x) uniformized to the length scale of the diffusion/reaction $L_t(L_t = \sqrt{D^*/k^*} = 0.3\ mm)$. Pe_t is the Peclet number which observes the significance of convection effect on diffusion in the tumor tissue. For carmustine, Pe_t is 0.06. $v_c = 1 \times 10^{-7}\ (m/s)$ is the characteristic velocity in both remnant tumor and nearby normal tissue.

The boundary conditions contain: (i) the agent concentration is 1 at the beginning of penetration in the cavity/remnant interfacial surface $(\Gamma_t = 1 \text{ for } \xi = 0)$, (ii) the agent concentration is nearly 0 at infinite site $(\Gamma_t = 0 \text{ for } \xi = \infty)$. Hence, for the velocity (v_x) is an unchanged parameter, the form of solution can be expressed by following:

$$\Gamma_t = e^{(p-\sqrt{1+p^2})\xi}, \tag{40}$$

where $p = v_x/2\sqrt{k^*D^*}$. p reflects the importance of convection influencing carmustine penetration [6, 7].

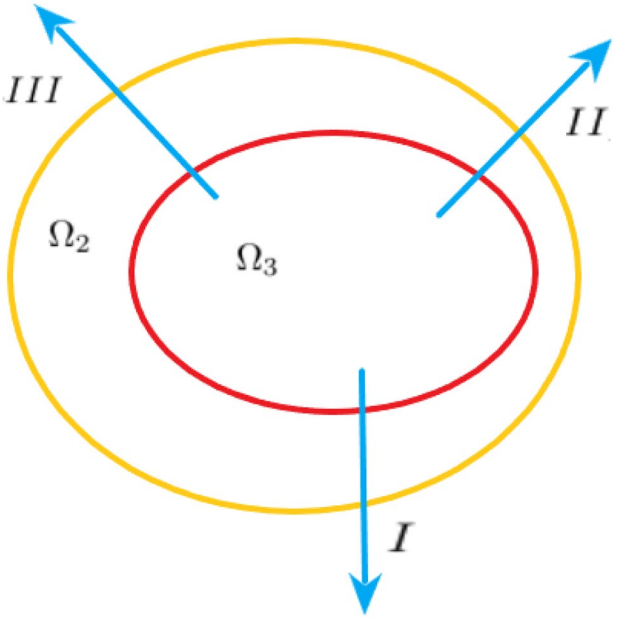

Fig. 8 The direction of three different lines to show the convection flow

Figure 9 compares the numerical solutions about Γ_t versus the penetration distance (x/L, here L is 2.3 mm, which represents the thickness of the remnant tumor,). For line I ($p = 0.12$), convection can stretch the distance of penetration enhancing drug penetration, compared with the pure diffusion and reaction. It seems to be the opposite for line III ($p = -0.18$), where the penetration could be repressed by convection due to the concentration is nearly 0 at the end of the boundary. Along line II ($p = 0.02$), the penetration is mainly influenced by diffusion or reaction [7]. Nonetheless, the convection effect slightly on the concentration profiles, which means that carmustine transport is dominated by diffusion. However, the numerical results are not totally accurate because the assumption of the tumor is infinite. In the normal tumor, there will be a boundary $\partial\Omega_2$ to control the decreasing concentration.

In dimensionless analysis, the value of relevant parameters, like Γ_t and ξ, are strictly set to be between 0 and 1 for the purpose of obtaining the more intuitive picture. Otherwise, it would not be linear. In order to show the two-dimensional simulation in the remnant tumor, it is assumed that there is a steady concentration on the boundary between cavity and remnant tumor which is a semiannular region, and the inner part is the cavity. Because of the Peclet number $Pe_t = 0.06$ in remnant tumor is much less than the $Pe_c = 2$ [6], the convection in this result is not as obvious as former study, the prominent part is the diffusion term which can be showed by Fig. 10.

Combining with the simulation in the Fig. 7, it is almost certainly that the drug will release to a specific direction due to the influence of diffusion convection and reaction. In the actual administration of the drug, it may produce a better effect by following the integrate direction.

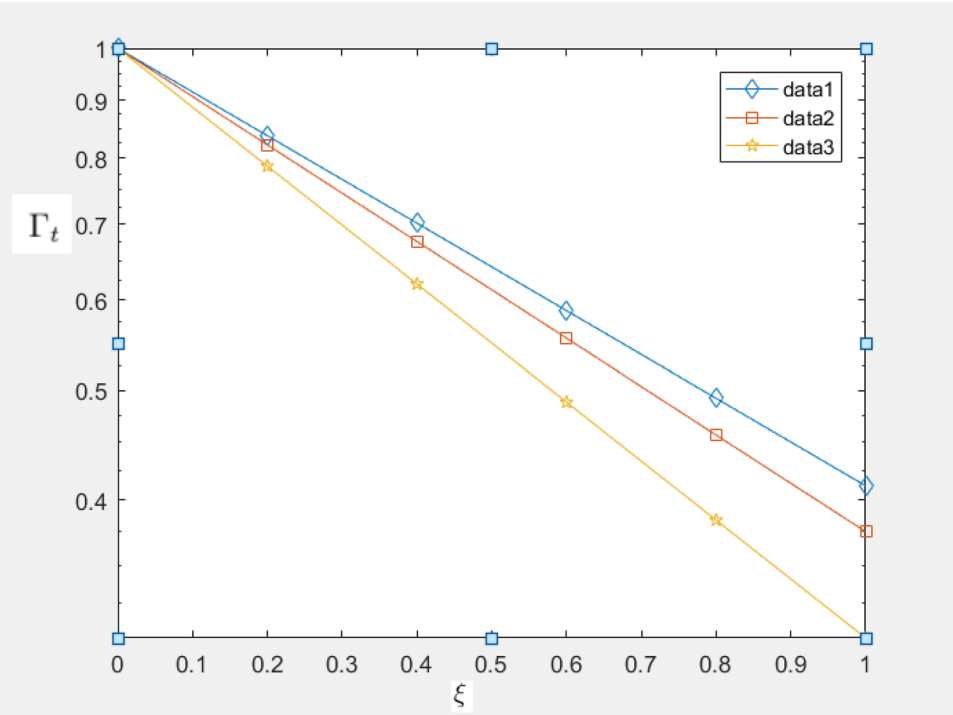

Fig. 9 The carmustine penetration among line I, (i.e. data 1), line II, (i.e. data 2), line III, (i.e. data 3). The concentration is from 0 to above 0.4 along line I, for line II, the concentration is below the 0.4, and it is nearly 0 when ξ is closed to 1 due to the inhibiting effect of convection

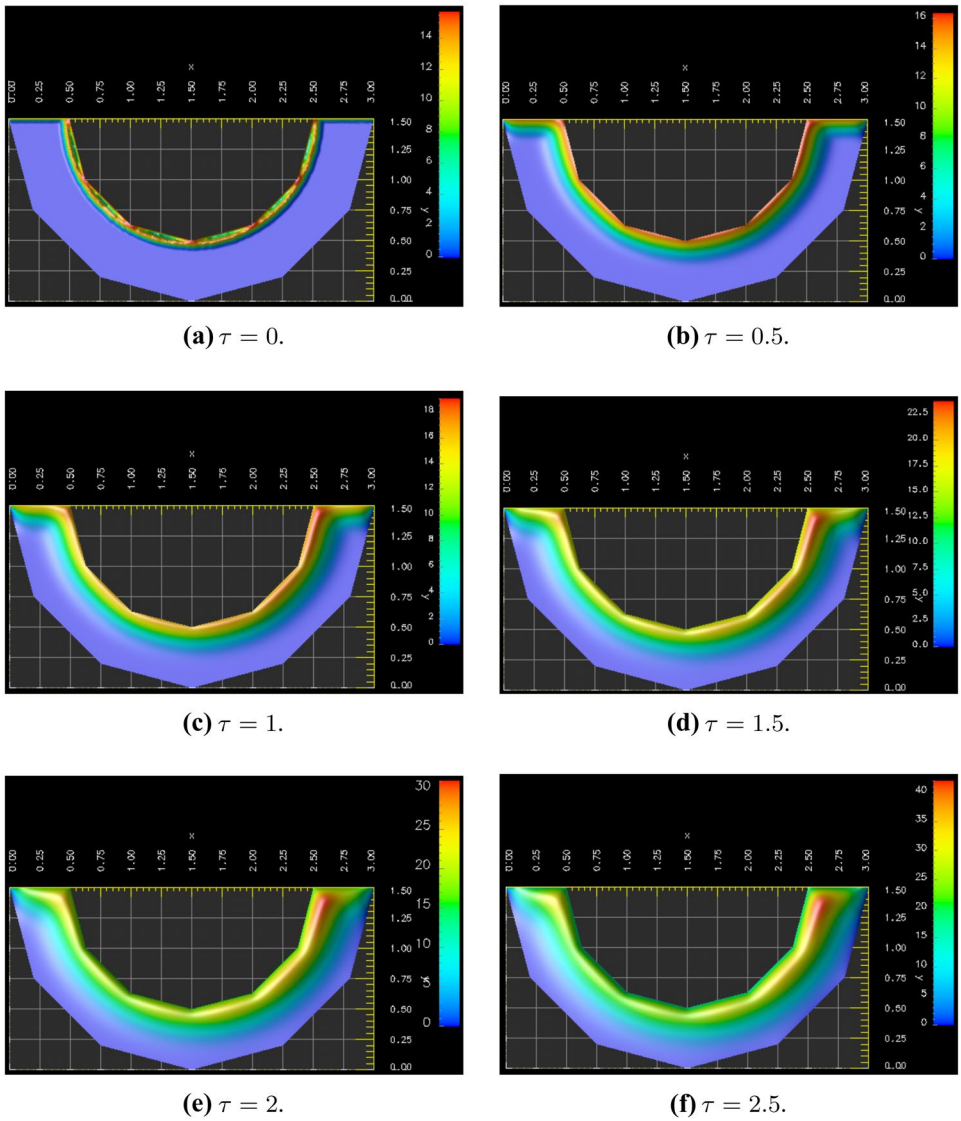

(a) $\tau = 0.$ **(b)** $\tau = 0.5.$ **(c)** $\tau = 1.$ **(d)** $\tau = 1.5.$ **(e)** $\tau = 2.$ **(f)** $\tau = 2.5.$

Fig. 10 The change from boundary between the cavity and remnant tumor to the outer tumor layer with τ from 0 to 2.5

The convection affected by two drugs in monkey brain

In the previous research, the site of the drug was gained by scanning the coronal plane and the concentration was estimated from the edge of the polymer implant at different days [25]. it may reduce the influence of drug penetration by convection because the fluid flow is from the ventricle to the outer boundary of the brain. Also, all tests here were proceeded in normal tissue. Figure 11 shows the concentration of two drugs in numerical data calculated by Eq. (40) comparing with the experimental statistics which are gained from monkey brain [25]. Y is the dimensionless concentration in the normal tissue, and $\mathrm{X} = x_n/L_n$ represents the dimensionless distance from the surface of the polymer pellet in the normal brain. where $L_n = 0.3mm$ is the diffusion/reaction length scale. In Fig. 11(a), as p is between 0.8 and 2.2, the convection would exist in the monkey brain [6]. The penetration of carmustine is heightening on day 7 and day 14 ($p = 2.2$), and it is not obvious on day 30 ($p = 0.8$). This may be influenced by the vanishment of the edema or the rate of drug penetration is retarded. For Fig. 11(b), $p^{'}$ is the importance of convection influencing paclitaxel penetration with the fitted value from -0.5 to 0.3, the penetration of paclitaxel in day 1 ($p^{'} = -0.5$) is more enhanced than the data in day 3 and day 5 ($p^{'} = 0.3$), this may advice that the velocity of paclitaxel penetration is larger than carmustine, or it is influenced rarely by the edema. In the numerical solution, the more enhanced penetration will be obtained if the p or $p^{'}$ is larger.

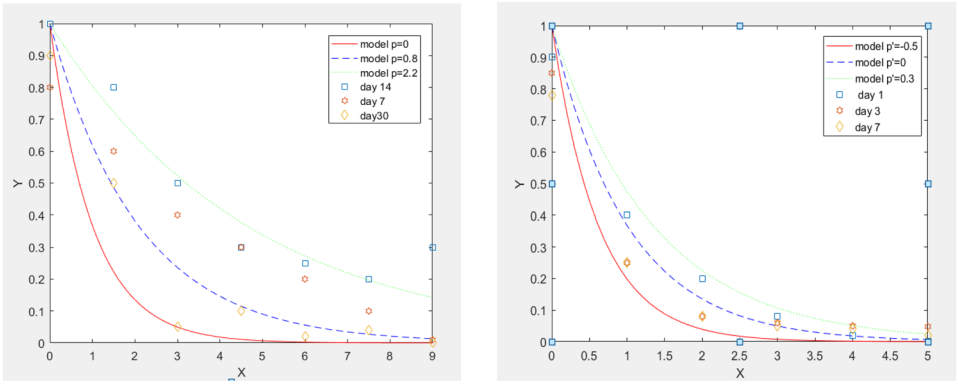

(a) (b)

Fig. 11 (**a**) carmustine. (**b**) paclitaxel. The numerical models of penetration of two drugs compared with the experimental statistics, respectively. The Y represents the dimensionless concentration in the normal tissue, and the X represents the dimensionless distance from the surface of the polymer pellet

Conclusion

This study explores the concrete simulation (pressure, concentration) in the brain tumor, which demonstrates that numerical methods are effective ways to combine with the process of drug release and provides a mechanistic explanation for clinical tests. Although diffusion is the dominant transportation way, the influence of the convection is significant, especially in the remnant tumor after surgery due to the concentration moves to a nearly fixed direction. Besides, these simulation results can be regarded as a guide for remedy optimization and dynamic analysis of other drugs (paclitaxel) for tumor treatment. Moreover, the mathematical model may have a wide application on drug release in multiple dosage forms, such as long sustained release microspheres, oral extended release hydrophilic matrix tablets, hydrogel, and sustained release topical rings.

Acknowledgements Current research is financially supported by the Macau FDCT Research Grant (FDCT/0029/2018/A1) and the University of Macau Research Grant (MYRG2019-00041-ICMS), and the research of the second author is funded by National Natural Science Foundation of China via 11922120 and 11871489.

Author contributions Defang Ouyang and Guanghui Hu designed and directed the project; Chen Hongyu made the simulations; Chen Hongyu, Defang Ouyang and Guanghui Hu wrote the article.

Funding Current research is financially supported by the Macau FDCT Research Grant (FDCT/0029/2018/A1) and the University of Macau Research Grant (MYRG2019-00041-ICMS).

Data availability All data will be available under request.

Code availability The code will be available under request.

Declarations

Ethics approval Not applicable.

Consent to participate Not applicable.

Consent for publication All authors agreed to publication in DDTR.

Conflicts of interest There are no conflicts of interest.

References

1. GBD 2016 Neurology Collaborators. Global, regional, and national burden of the brain and other CNS cancer, 1990–2016: a systematic analysis for the Global Burden of Disease Study 2016. Lancet Neurol. 2019;18(5):459–480.
2. Park BJ, Kim HK, Sade B, Lee JH. Epidemiology. In: Lee JH, editor. Meningiomas: Diagnosis, Treatment, and Outcome. Springer; 2009. p. 11. ISBN 978-1-84882-910-7.
3. Herholz K, Langen K-J, Schiepers C, Mountz JM. Brain Tumors. Semin Nucl Med. 2012;42(6):356–70.
4. Adult Brain Tumors Treatment. NCI. 2014-02-28. Retrieved 8 June 2014.
5. Brem H, Gabikian P. Biodegradable polymer implants to treat brain tumors. J Control Release. 2001;74:63–7.
6. Arifin DY, Lee KYT, Wang C-H, Smith KA. Role of Convective Flow in Carmustine Delivery to a Brain Tumor. Pharmaceutical Research. 2009;26(10).
7. Arifin DY, Lee KYT, Wang C-H. Chemotherapeutic drug transport to a brain tumor. J Control Release. 2009;137:203–10.
8. Balossier A, Dorner L, Emery E, Heese O, Mehdorn HM, Menei P, Singh J. Incorporating BCNU Wafers into Malignant Glioma Treatment. Clin Drug Investig. 2010;30(3):195–204.
9. Engelhard HH. The role of interstitial BCNU chemotherapy in the treatment of malignant glioma. Surg Neurol 2000;53:458–64.
10. Sefidgar M, et al. Effect of tumor shape, size, and tissue transport properties on drug delivery to solid tumors. J Biol Eng. 2014;8(1):1–13.
11. Saltzman WM, Radomsky ML. Drugs released from polymers: diffusion and elimination in brain tissue. Chem Eng Sci. 1991;46:2429–44.
12. Fung LK, Shin M, Tyler B, Brem H, Saltzman WM. Chemotherapeutic drugs released from polymers: distribution of 1,3-bis(2-chloroethyl)-1-nitrosourea in the rat brain. Pharm Res. 1996;13:671–82.
13. Kalyanasundaram S, Calhoun VD, Leong KW. A finite element model for predicting the distribution of drugs delivered intracranially to the brain. Am J Physiol Regul Integr Comp Physiol. 1997;42:R1810–21.

14. Wang CH, Li J, Teo CS, Lee T. The delivery of BCNU to brain tumors. J Control Release. 1999;61:21–41.
15. Tan WHK, Wang F, Lee T, Wang CH. Computer simulation of the delivery of etanidazole to brain tumor from PLGA wafers: comparison between linear and double burst release systems. Biotechnol Bioeng. 2003;82:278–88.
16. Eikenberry Steffen. A tumor cord model for doxorubicin delivery and dose optimization in solid tumors. Theor Biol Med Model. 2009;6(1):1–20.
17. Li R. On multi-mesh h-adaptive methods. J Sci Comput. 2005;24(3):321–41.
18. Weller RO, Djuanda E, Yow H-Y, Carare RO. Lymphatic drainage of the brain and the pathophysiology of neurological disease. Acta Neuropathol. 2009;117(1).
19. Li B, Liu XJ, Li L, Zhang SH, Li Y, Li DD, Zhen YS. A tumor-targeting dextran-apoprotein conjugate integrated with enediyne chromophore shows highly potent antitumor efficacy. Polym Chem. 2014;5(19):5680–8.
20. Baxter LT, Jain RK. Transport of fluid and macromolecules in tumors. I. Role of interstitial pressure and convection. Microvasc Res. 1989;37:77–104.
21. Less JR, Skalak TC, Sevick EM, Jain RK. Microvascular architecture in a mammary carcinoma: branching patterns and vessel dimensions. Cancer Res. 1991;51:265–73.
22. Zhan W, Wang C-H. Convection enhanced delivery of chemotherapeutic drugs into brain tumor. J Control Release. 2018;271:74–87.
23. Wang C-H, Li J. Three-dimensional simulation of IgG delivery to tumors. Chem Eng Sci. 1998;53:3579–600.
24. Torres AJ, Zhu C, Shuler ML, Pannullo S. Paclitaxel delivery to brain tumors from hydrogels: a computational study. Biotechnol Prog. 2011;27(5):1478–87.
25. Fung LK, Ewend MG, Sills A, Sipos EP, Thompson R, Watts M, Colvin OM, Brem H, Saltzman WM. Pharmacokinetics of interstitial delivery of carmustine, 4- hydroperoxy cyclophosphamide, and paclitaxel from a biodegradable polymer implant in the monkey brain. Cancer Res. 1998;58:672–84.
26. Eikenberry S. A tumor cord model for doxorubicin delivery and dose optimization in solid tumors. Theor Biol Med Model. 2009;6:16.
27. Zhan W, Arifin DY, Lee TKY, Wang C-H. Mathematical Modelling of Convection Enhanced Delivery of Carmustine and Paclitaxel for Brain Tumour Therapy. Pharm Res. 2017;34:860–73.
28. Goodman Gilman A, Rall RW, Nies AS, Taylor P. Goodman and Gilman The Pharmacological Basis of Therapeutics. 8th ed. New York: Pergamon; 1990. p. 1221.
29. Zhan W. Delivery of liposome-encapsulated temozolomide to brain tumor: Understanding the drug transport for optimization. Int J Pharm. 2019;557:280–92.
30. Kilberg HK. Water homeostasis in the brain: basic concepts. Neuroscience. 2004;120:852–60.
31. Rapoport SI. A mathematical model for vasogenic brain edema. J Theor Biol. 1978;74:439–67.
32. Green DW, Perry RH. Perry's Chemical Engineers' Handbook/ edicion Don W, Greeny Robert H, Perry; 1973.
33. Kimelberg HK. Water homeostasis in the brain: basic concepts. Neuroscience. 2004;120:852–60.
34. Wolff JE, Berrak S, Webb SEK, Zhang M. Nitrosourea efficacy in high-grade glioma: a survival gain analysis summarizing 504 cohorts with 24193 patients. J Neuro-Oncol 2008;88:57–63.
35. Fleming AB, Saltzman WM. Pharmacokinetics of the carmustine implant. Clin Pharmacokinet. 2002;41:403–19.
36. Gross JF, Popel AS. Mathematical Models of Transport Phenomena in Normal and Neoplastic Tissue. Boca Raton, FL, USA: CRC Press; 1979.